



Low surface strength of the asteroid Bennu inferred from impact ejecta deposit

M. E. Perry ¹ ¹ ², O. S. Barnouin ¹, R. T. Daly ¹, E. B. Bierhaus ¹, R.-L. Ballouz ¹, K. J. Walsh ¹, M. G. Daly ¹, D. N. DellaGiustina ¹, M. C. Nolan ¹, J. P. Emery ¹, M. M. Al Asad ¹, C. L. Johnson ⁷, C. M. Ernst ¹, E. R. Jawin ⁸, P. Michel ¹, D. R. Golish ¹, W. F. Bottke ¹, J. A. Seabrook ¹ and D. S. Lauretta ¹

The surface strength of small rubble-pile asteroids, which are aggregates of unconsolidated material under microgravity, is poorly constrained but critical to understanding surface evolution and geologic history of the asteroid. Here we use images of an impact ejecta deposit and downslope avalanche adjacent to a 70-m-diameter impact crater on the rubble-pile asteroid (101955) Bennu to constrain the asteroid's surface properties. We infer that the ejecta deposited near the crater must have been mobilized with velocities less than Bennu's escape velocity (20 cm s⁻¹); such low velocities can be explained only if the effective strength of the local surface is exceedingly low, nominally ≤2 Pa. This value is four orders of magnitude below strength values commonly used for asteroid surfaces, but it is consistent with recent estimates of internal strength of rubble-pile asteroids and with the surface strength of another rubble-pile asteroid, Ryugu. We find a downslope avalanche indicating a surface composed of material readily mobilized by impacts and that has probably been renewed multiple times since Bennu's initial assembly. Compared with stronger surfaces, very weak surfaces imply (1) more retention of material because of the low ejecta velocities and (2) lower crater-based age estimates—although the heterogeneous structure of rubble piles complicates interpretation.

he surface of a planetary body reflects its evolution, impact history, degradation processes and material properties. Of importance to interpreting remote observations of such bodies is the surface's resistance to mechanical changes, represented by a group of properties described as 'strength', defined as the ratio between a resisting force or applied load and the cross-sectional area, in units of stress (pascals (Pa)). Using only Earth-based observations, determining the surface strength of a distant asteroid is challenging, especially in the case of small rubble-pile asteroids that consist of gravitationally bound, unconsolidated fragments of collisionally disrupted precursors1. For calculating crater-retention age in such cases, it has been common to assume a surface strength >100,000 Pa, typical of weakly cemented basalt² and lunar regolith³. Although these are reasonable proxies, they are disconnected from recent, much lower estimates of the internal strength of rubble-pile asteroids⁴.

The Hayabusa2 and OSIRIS-REx (Origins, Spectral Interpretation, Resource Identification and Security–Regolith Explorer) missions to the rubble-pile asteroids Ryugu⁵ and Bennu^{6,7}, respectively, have offered the opportunity to constrain surface strength via space-craft data acquired in proximity. OSIRIS-REx observations of the ~500-m-diameter Bennu⁶ have shown that its metre-scale boulders have an estimated strength of 0.1–1.7 MPa (refs. ^{8,9}), but this does not tell us about the inter-particle cohesive strength that is relevant for the response of loose regolith to impact cratering. Analyses of Hayabusa2's Small Carry-on Impactor (SCI) experiment¹⁰ on Ryugu, in which a 15-m-diameter crater was artificially created, suggest

an exceptionally low surface strength of <1.3 Pa. However, it is not clear whether the low strength implied from this single experimental outcome can be extrapolated to larger craters, to the global surface of Ryugu or to other rubble-pile asteroids. In this article, we use OSIRIS-REx observations to investigate the surroundings of a larger natural-impact crater on Bennu, with implications for surface strength and the generalizability of the SCI experimental result.

An ejecta field on Bennu

In images of Bennu acquired by the OSIRIS-REx Camera Suite (OCAMS)¹¹⁻¹³, we observed an unusually smooth, homogeneous area surrounding and downslope (north) of the 70-m-diameter Bralgah Crater (Fig. 1a) centred at -45°, 325°E. (Here, slope is the angle between the surface normal and the gravity vector, with lower elevations downslope.) The terrain is the largest photometrically distinct and smooth area on Bennu (Fig. 1b-d and Extended Data Fig. 1), encompassing ~0.024 km² or 6% of the southern hemisphere. In multispectral images, the colour of the crater and the surrounding smooth area is more homogeneous than that of the rest of Bennu's surface (Fig. 1d and Extended Data Fig. 1), which varies at the scale of boulders (metres to tens of metres)¹⁴. This region shows a distinct b'/v normalized band ratio >1 (where b' is $0.44-0.50 \,\mu m$ and ν is 0.52-0.58 µm). Previous work associated high b'/ν band ratios with younger, smoother terrains on Bennu, including those that might have experienced recent mass movement¹⁴. The surface is twice as smooth as the Bennu average in measures of roughness such as variations in slope over length scales of 1 to 5 m (ref. 15)

¹Johns Hopkins University Applied Physics Laboratory, Laurel, MD, USA. ²Lockheed Martin Space, Littleton, CO, USA. ³Lunar and Planetary Laboratory, University of Arizona, Tucson, AZ, USA. ⁴Southwest Research Institute, Boulder, CO, USA. ⁵The Centre for Research in Earth and Space Science, York University, Toronto, Ontario, Canada. ⁴Department of Earth and Planetary Sciences, University of Tennessee, Knoxville, TN, USA. ¹Department of Earth, Ocean and Atmospheric Sciences, University of British Columbia, Vancouver, British Columbia, Canada. ⁴National Museum of Natural History, Smithsonian Institution, Washington, DC, USA. ⁴Université Côte d'Azur, Observatoire de la Côte d'Azur, CNRS, Laboratoire Lagrange, Nice, France. ™e-mail: mark.perry@jhuapl.edu

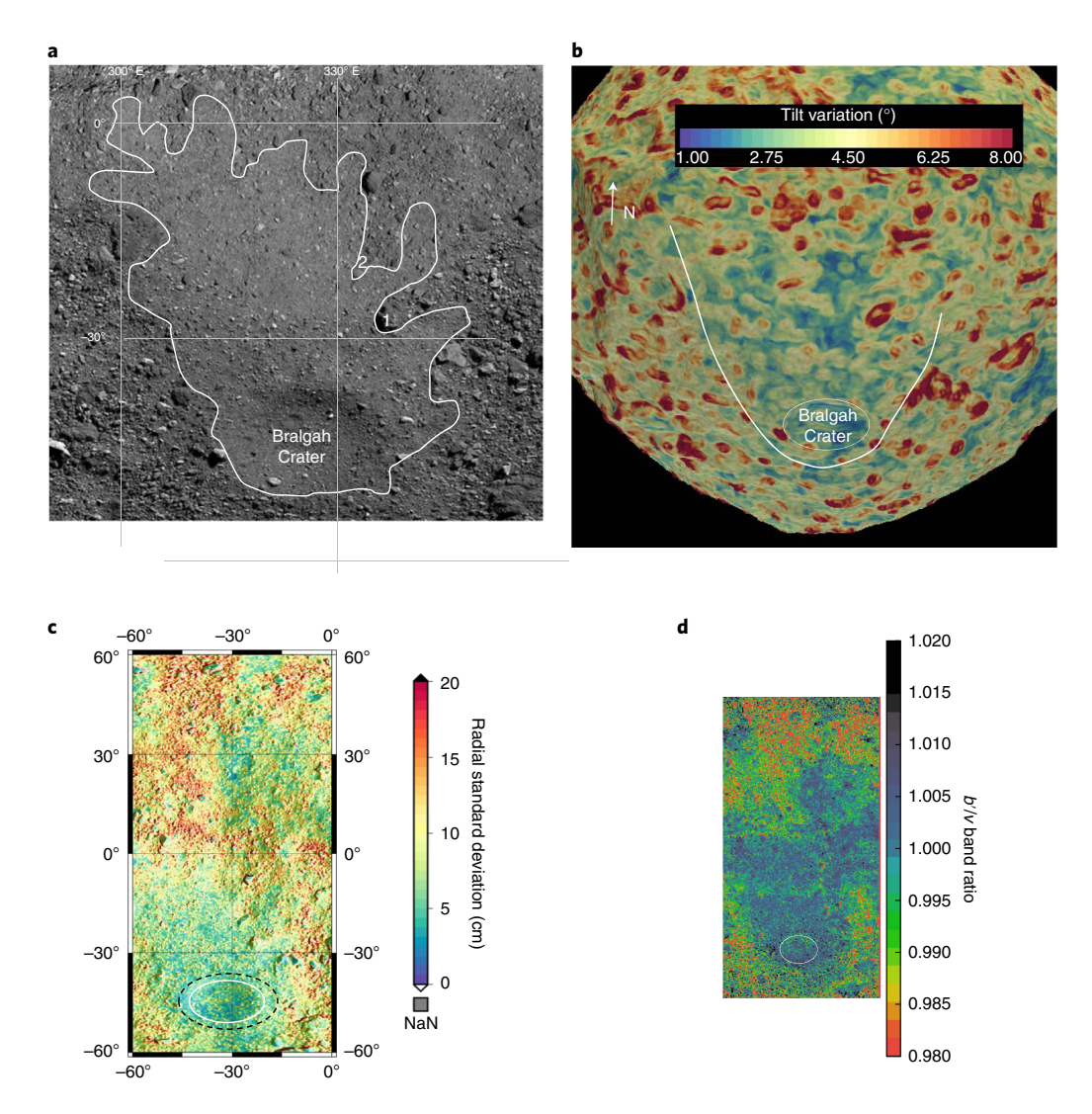


Fig. 1 | Bralgah Crater and the surrounding uniform terrain. \mathbf{a} , OCAMS PolyCam mosaic¹³ showing the uniform terrain (white border) northward of and surrounding the 70-m-diameter crater. The terrain northeast of the two rocks labelled 1 and 2 (-20° , 333° E and -28° , 337° E) is rougher and darker. The top of this image is just north of the equator, where elevations are lowest on Bennu. \mathbf{b} , Tilt variation, a measure of surface roughness, showing the range of surface slopes within the local area. \mathbf{c} , Surface roughness from OSIRIS-REx Laser Altimeter measurements. The colours represent the standard deviation of the radii of all laser altimeter measurements within 80 cm facets. The black dashed line marks a smooth area surrounding the crater. \mathbf{d} , The b'/v band ratio map for 300° E to 0° and -60° to 60° latitude. Bralgah Crater and the surrounding terrain have higher ratios.

and tilt variation (Fig. 1c). There are two boulders to the northeast (Fig. 1a), beyond which the terrain farther from the crater is rockier and 2 to 5 m lower in elevation (Extended Data Fig. 2).

The crater itself is encircled by a well-defined raised rim and has a slightly asymmetric bowl-shaped interior (Extended Data Fig. 3) 16 . Among similarly sized craters on Bennu 16 , Bralgah Crater's morphology is most reminiscent of classical craters on larger bodies such as Earth's Moon. The well-defined topographic expression and morphology suggest that Bralgah Crater has undergone little degradation 16 . It has a rim-to-floor depth/diameter ratio of 0.07 ± 0.01 with respect to elevation and a volume of 9×10^3 m $^3 \pm 50\%$ (ref. 16). The crater resides on an ~23° regional slope. The northern crater wall has a steeper slope than the southern wall, which has more large boulders.

Buried structures near the surface can complicate crater formation ^{10,16}, but there is no evidence of this at Bralgah Crater. Its circular rim and relatively smooth floor indicate that the near-surface material was initially uniform and did not contain large boulders or regions of higher strength to interfere with crater formation. To

achieve this uniformity, the homogeneity of the near-surface material at the location of Bralgah Crater would need to extend to a depth of approximately a tenth of a crater diameter, or 7 m. Given the rough and varied surface of Bennu⁶, this homogeneity is initially surprising. However, it is supported by two other observations: (1) the crater is located in the southern hemisphere, where the preponderance of large boulders appears to impede the downslope flow of regolith toward the equator, effectively retaining more fine material in this hemisphere^{17,18}, and (2) localized mass flows have excavated up to about 10 m of regolith from around large boulders on Bennu¹⁸, suggesting a reservoir of mobile material.

Because the smooth, uniform terrain surrounds and inhabits the crater, we infer that they formed concurrently. A crater that post-dated the terrain would have distinct roughness and colour, and a crater that pre-dated it would show evidence of infilling, particularly at the downslope crater wall, which would be shallower than the upslope wall instead of steeper as we observe. We therefore conclude that the material that composes the uniform terrain is a product of or triggered by the cratering event.

Table 1 | Scaling relationships for both gravity and strength regimes used for calculations and simulations of impact cratering and resulting ejecta

Parameter	Values and relationships
Crater radius (strength regime)	$R\left(\frac{\rho}{m}\right)^{1/3} = H_2\left(\frac{\rho}{\delta}\right)^{(1-3\nu)/3} \left[\frac{\gamma}{\rho U^2}\right]^{-\mu/2}$
Crater radius (gravity regime)	$R\left(\frac{\rho}{m}\right)^{1/3} = H_1\left(\frac{\rho}{\delta}\right)^{(2+\mu-6\nu)/[3(2+\mu)]}\left[\frac{g\sigma}{U^2}\right]^{-\mu/(2+\mu)}$
Transition strength (Y _t)	$Y_{\rm t}=\rho ga$ (The gravity regime applies when surface strength is less than $Y_{\rm t}$; for Bennu, $Y_{\rm t}$ <1Pa for a <1m)
Ejection velocity (strength regime)	$v\sqrt{\frac{\rho}{\gamma}} = C_3 \left(\frac{x}{R}\right)^{-1/\mu} C_3 = C_1 \left((4\pi/3)^{1/3} H_2\right)^{-1/\mu}$ At the crater radius, $(x=R)$ simplifies to $v \sim = \sqrt{Y/\rho}$
Ejection velocity (gravity regime)	$\frac{v}{\sqrt{gR}} = C_2 \left(\frac{x}{R}\right)^{-1/\mu} C_2 = C_1 \left((4\pi/3)^{1/3} H_1 \right)^{-(2+\mu)/2\mu}$ At the crater radius, $(x=R)$ simplifies to $v \sim = \sqrt{gR}$
Mass ejected faster than $v(M(v))$; strength regime)	$\frac{M(v)}{\rho R^3} = C_6 \left(v \sqrt{\frac{\rho}{\gamma}} \right)^{-3\mu} C_6 = C_4 H_2^{-3}$
Mass ejected faster than v (gravity regime)	$\frac{M(v)}{\rho R^3} = C_5 \left(\frac{v}{\sqrt{gR}}\right)^{-3\mu} C_5 = C_4 (4\pi/3)^{-\mu/2} H_1^{-3(\mu+2)/2}$
Target parameters (varied)	Density $(\rho) = [1,000 \text{ to } 1,500] \text{ kg m}^{-3}, Y = [0 \text{ to } 100]$
Impactor parameters, gravity regime (varied)	Density (δ) = [1,500 to 3,600] kg m ⁻³ , U = [3,000 to 7,000] m s ⁻¹ , a = [0.17 to 1.3] m
Bennu parameters	$GM = 4.93 \text{m}^3 \text{s}^{-2}$, rotation period = 4.3 h, shape model v42, steepest slopes = 40°
Modification factor for velocity near crater edge	$\left(1 - \frac{x}{n_2 R}\right)^p$ with $n_2 = 1.3$ and $p = 0.3$ for the gravity regime
Mass ejected from inside x	$M(x) = k\rho x^3$ with $k = 0.3$ for the gravity regime

R is the final crater radius; Y is a measure of surface strength (Pa); ρ is surface density; U, δ and m, respectively, are impactor velocity, density and mass; a is the impactor radius; x is the radial distance from the crater centre; ν , μ , C_{ν} , C_{α} , H_{ν} , ρ , P_{α} , k and H_{2} are fitted constants (Extended Data Table 1).

The smooth region is asymmetric as expected for an ejecta deposit on a sloped terrain: material ejected downslope (in this case, north) would travel farther and land with a higher-velocity component along the surface than material ejected in other directions, leading to the northward elongation we observe (Fig. 1). Material ejected upslope (south) would land with a velocity near normal incidence and have less than 1 cm s⁻¹ velocity along the surface. Much of the ejecta on the upslope side of the crater would land closer to the upslope (southern) crater rim, consistent with the limited extent of the smooth region south of the crater (Fig. 1). Experiments¹⁹ suggest that upslope ejecta would probably have collapsed into the crater shortly after landing, contributing to the observed shallower slope of the southern crater wall. Further, the uniform ring of terrain on and just beyond the rim, uphill and to the south, east and west (Fig. 1a), is best explained by material that left the crater in those directions rather than by mass wasting, which would create only downslope movement (compare refs. 18,20). We thus infer that the uniform terrain consists of ejecta from the impact that formed Bralgah Crater.

Ejecta and surface strength

For ejecta to fall back onto Bennu's surface, the particles must be ejected at speeds lower than Bennu's escape velocity of $20 \, \text{cm/s}^{-1}$ (refs. 21,22). Impact-scaling relationships (Table 1), developed from terrestrial testing and combined with assumptions about impact velocity and material properties, enable parameters such as ejecta velocities to be estimated from the crater size^{23,24} (Methods). The stronger and more cohesive the surface material, the higher the ejection velocities²⁴.

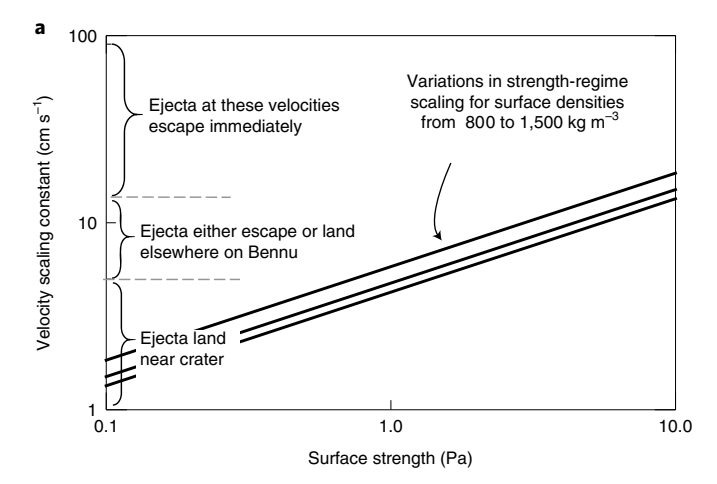
Analyses of crater formation are typically parameterized in either a strength or gravity regime (a third regime, armouring, where the impactor is smaller than the target surface particle, inhibits crater formation and instead disrupts the target particle²⁵). In the strength regime, surface strength controls the impact process, particularly the crater/impactor size ratio and the velocities of the ejecta. If strength is negligible, then ejecta velocities and the final crater size are controlled only by gravity. Heretofore, it was reasonable to assume that

all craters on Bennu formed in the strength regime because so little strength would be needed to exceed the influence of the microgravity of such a small asteroid: surface accelerations on Bennu range from $5 \times 10^{-5} \,\mathrm{m} \,\mathrm{s}^{-2}$ at the equator to $8 \times 10^{-5} \,\mathrm{m} \,\mathrm{s}^{-2}$ at the poles²¹.

For either regime, most mass is ejected late in crater formation from near the crater edge, where ejecta velocities are also lowest (Fig. 2b). The scaling relationship for a gravity-controlled impact is $v = C_2 \sqrt{gR}$, where v is the ejection velocity for material near the crater edge, g is the local acceleration of gravity, R is the final crater radius and C_2 is a fitted constant²⁴. For Bralgah Crater, an impact in the gravity regime would produce ejecta with $v = 2.2 - 2.8 \, \mathrm{cm} \, \mathrm{s}^{-1}$ near the crater edge, resulting in suborbital particle trajectories that re-impact Bennu within a crater diameter, as seen in simulations of the ejecta trajectories (Fig. 3 and Methods).

To find strengths consistent with ejecta observed near Bralgah Crater, we examine the effect of surface strength on the distribution of ejecta speeds. Cohesion and surface strength inhibit the ejection process such that ejected particles have higher velocities². Our analyses reveal that a minuscule surface strength of more than a few pascals would cause most material to leave the crater with velocities higher than those of gravity-regime ejecta and higher than the ~2.8 cm s⁻¹ required for ejecta to land near the crater (Fig. 2 and Extended Data Fig. 4). Depending on the fitted parameters, which are based on a range of materials used in terrestrial experiments, the surface strength that matches the mass versus velocity distribution of ejecta in the gravity regime is 0.1 to 2.0 Pa. At higher strengths, some ejecta can still land near the crater, but above 100 Pa, nearly all ejecta escape; we thus consider 100 Pa to be an extreme upper bound.

The nominal strength of 0.1 to 2 Pa is substantially below most material analogues used in crater studies. Dry soils on Earth and loose lunar soils have respective strengths of 180 kPa² and >520 Pa²6. If these strength values existed on Bennu, the ejecta from Bralgah Crater would have launched at velocities much higher than the asteroid's escape velocity. Thus, the presence of ejecta surrounding Bralgah Crater demonstrates that crater formation can be controlled by extremely low or negligible strength (the gravity regime)



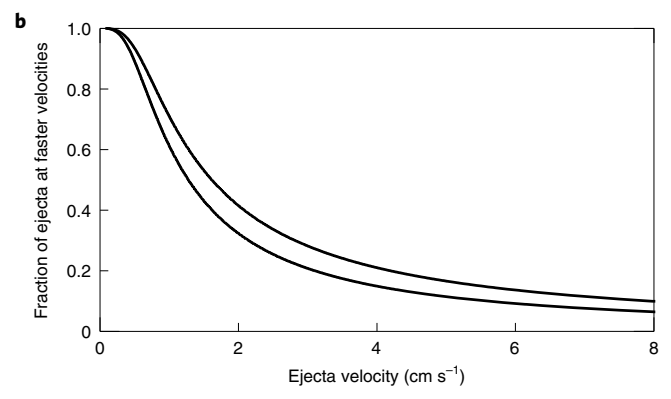


Fig. 2 | Relationships between the mass and velocity of ejecta from scaling relationships. a, Ejecta velocities increase with surface strength proportional to the velocity scaling constant, $C_3 \sqrt{Y/\rho}$. If strength is greater than a few pascals on Bennu, then most of the ejecta, which are launched near the crater edge, will either land far from the crater or escape (the dashed lines indicate these transitions). Variations due to the unknown density of the upper 7 m of regolith on Bennu represent uncertainty in the mass-velocity relationship, shown for a sand/fly-ash mixture²⁴. Variations in the microgravity crater-forming processes at the crater edge due to differing material properties are much larger and discussed in Methods. **b**, During a cratering event, most mass is ejected at lower speeds and near the crater edge. Using the size of Bralgah Crater, gravity-regime scaling, parameters derived from experiments (Extended Data Table 1) and the modification factor for velocity near the edge (Methods), this plot shows the fraction of total ejected mass that has speeds above the plotted values. The difference between the two curves, one using parameters for sand (upper curve) and one for glass microspheres (lower curve), is a proxy for the uncertainty in the massvelocity relationship in the gravity regime; 10% or less of the ejected mass is ejected faster than 8 cm s⁻¹.

on rubble-pile bodies. This conclusion is supported by the very low effective strength (<1.3 Pa) deduced from Hayabusa2's SCI artificial cratering experiment on Ryugu¹⁰.

Evidence of surface mass flow

The depression in elevation behind (north of) boulder 2 in Fig. 1 and Extended Data Fig. 2 is 4–5 m deep and provides an estimate of the thickness of the smooth terrain north and downhill of Bralgah Crater. If material excavated from the crater were uniformly distributed over this terrain, it could account for only 20–30 cm of that thickness. Moreover, the majority of ejecta would re-impact Bennu within one crater diameter from the rim (see the dense region near

the crater rim in Fig. 3a), whereas the observed deposit extends to the equator, almost three times farther. Some of this material appears to have flowed up to and around boulders 1 and 2 (Fig. 1). Ejecta deposition alone would have placed particles both atop and downslope of the boulders, which we do not observe. Images show that material flowed north–northwest¹⁸ as it piled against the boulders (Extended Data Fig. 5). These observations suggest that a mass flow field added material to the elongated ejecta blanket.

The flow field and ejecta blanket are probably related. Downslope ejecta would have re-contacted Bennu at relatively shallow angles of 25° to 30° to the surface and with velocities of 5 to 7 cm s⁻¹ tangent to the surface (Fig. 3b). At our inferred low surface strength, this velocity is sufficient to dislodge particles. The material in this area exhibits a surface slope greater than 20° at Bennu's current rotation rate^{17,27}. This high slope angle suggests that the surface is marginally stable, and the returning ejecta would have been sufficient to supply what little impetus is required to initiate a downhill flow. Applying the scaling laws for impacts at very low speeds, a 10-cm-diameter ejecta particle returning to a strengthless surface at 5 cm s⁻¹ would create a 40-cm-diameter crater and activate a volume of material 100 times that of the particle. Repeated impacts of this nature could initiate large-scale mass wasting.

We considered seismic shaking²⁸ as a possible alternative mechanism for initiating the avalanche. However, because seismic shaking would have acted uniformly in all directions around the crater, an avalanche caused by this process would have started upslope of the crater and surrounded it, contrary to the downslope-only elongation that we observe (Supplementary Fig. 1). We therefore rule out seismic shaking as the dominant mechanism (see extended discussion in Supplementary Information).

Downslope flow has characteristics of a gravity current or inertial-debris flow, a granular flow composed of intensively colliding particles²⁹. Inelastic collisions of flowing particles and their plunge into the regolith provide momentum transport that entrains surface particles similarly to a powder-snow avalanche and differently from slumps or translational slides that do not engage as much underlying material. Inertial-debris flows may produce lobes, and we observe several such features at the northward terminus (Fig. 1a), with possible extension past the equator. For a portion of the field, no sharp demarcation is evident, which may be due to the flowing material slowing and thinning as it reaches the lower slopes near the equator. Large boulders are sometimes found at the terminus of mass wasting; the east-west cluster of boulders from 0° to 8° latitude may be such a collection (Fig. 1a). The lack of boulders larger than a few metres in the uniform terrain suggests that they have been removed or buried.

Static and dynamic friction angles in collections of particles supply coefficients that are useful for determining equivalent friction and its effect on flow. Bennu's steeper regional slopes are less than 40° (ref. 27), which is an upper bound for cohesionless material. Using 40° to represent the static friction angle, the estimated dynamic friction is $\sim\!10^\circ$ shallower (30°) and corresponds to a coefficient of dynamic friction of 0.58 (ref. 30). Applying this friction coefficient to the material disturbed by the returning ejecta, a flow that started with a velocity of 5 cm s $^{-1}$ would travel along a 20° slope more than 100 m, the distance to the equator, before being stopped by friction. A slightly lower dynamic friction angle of 25° requires only $3.5\,\mathrm{cm\,s^{-1}}$ initial velocity to reach the equator. For material moving at an angle to the slope, there is a slight downslope acceleration, but this has a small effect on the original velocity for material within 45° of the downslope direction.

With insufficient material available from the crater, most of the flow field must consist of existing, marginally stable regolith that was mobilized and remixed.

The flow must have been sufficiently massive to scour the surface over which it passed, removing unanchored rocks and leaving the

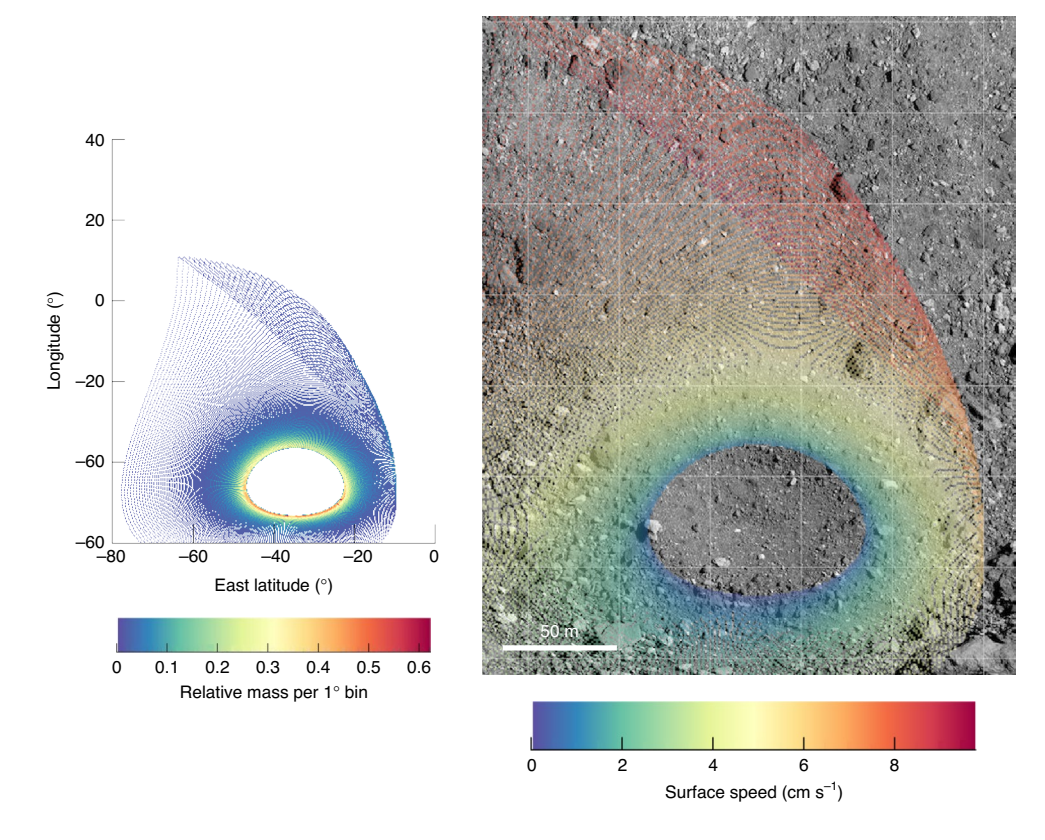


Fig. 3 | Simulation results of ejecta leaving the rim of Bralgah Crater according to gravity scaling. a, Density map of the mass deposition. The north/south asymmetry is due to the regional slope, and the westward curve is due to Bennu's rotation. **b**, Map of the ejecta collision velocity tangent to the surface as the ejecta re-impacts Bennu, overlain onto a map of the Bralgah Crater region. Ejecta that returns to the surface within a distance of one crater radius to the north lands with a velocity <3.5 cm s⁻¹. Material ejected at speeds between 8 and 12 cm s⁻¹ are omitted from the plots because their landed locations are widely dispersed over Bennu, and they make up less than 10% of the total ejected mass. Most material ejected at >12 cm s⁻¹ does not return to Bennu.

relatively smooth, homogeneous terrain that we observe. The lack of tracks from rolling boulders is not surprising if all of the material flowed together. Filling of low areas contributed to the observed smoothness of the terrain. Boulders 1 and 2 (Fig. 1) were too large or too deeply embedded to be dislodged. Disrupted material continued moving until it encountered an obstacle that it could not dislodge or reached the equatorial region, where elevation is lowest. The lack of secondary craters, which would normally be present around a large crater, is further corroboration of displacement due to flowing material.

A distinguishing characteristic of the impact that created Bralgah Crater is that it occurred in a deep reservoir of finer material. Most large craters on Bennu have rocky floors and shallow depth/diameter ratios, and some craters have central mounds, suggesting some strength at depth¹⁶. In those cases, gravity-scaled crater formation may have transitioned to the strength regime when encountering a coherent subsurface. The low ejection speeds that enabled ejecta retention in the case of the crater we studied would not have occurred. Given the extremely low-strength finding from the Hayabusa2 SCI experiment—as well as the compliant, viscous fluid-like response of Bennu's surface to contact by the OSIRIS-REx spacecraft during sample collection³¹—a reasonable conclusion is that an upper layer of fine material on rubble-pile asteroids such as Bennu and Ryugu is essentially strengthless but probably varies in thickness depending on the presence or absence of large (relative to the impactor) subsurface boulders within the cratering volume.

There are no other obvious, large ejecta fields on Bennu. Bralgah Crater is the only crater on Bennu with the necessary characteristics: large size (to provide sufficient material), mid-latitude location

(because material flows down towards the equator), impact into a deep layer of fine material (maintaining the gravity regime for the entire crater-forming event) and relative youth for a crater of its size (so that the field has not been overprinted and masked by subsequent surface processes). The flow field is highly visible because of the avalanche caused by the reaccreted ejecta. Most other large craters on Bennu are near or on the equator, so ejected material is already at low elevation and lands with negligible surface velocity. There are a few other large craters at high latitude, but they appear older and degraded²⁰, and it is possible that any associated ejecta or flow fields are weathered or disturbed past recognition.

Implications of a low-strength surface

The weaker the surface, the faster a body can be resurfaced. For the same population of impactors, crater radii in a strengthless surface are 10 times as large—involving 100 times the area and 1,000 times the volume—than surfaces responding in a strength regime with $Y \approx 0.2\,\mathrm{MPa}$. This difference is enhanced by ejecta retention: the low ejection velocities produced by impacts into low-strength surfaces return ejected material to the surface, modifying the top layer of the asteroid and infilling craters. From the ejecta-velocity equations (Table 1), most ejecta from impacts on Bennu are retained. For Bralgah Crater, >80% of the ejecta did not escape (Fig. 3 and Extended Data Fig. 4). An important consequence for rubble-pile asteroids is that their typically high spin rates create steep slopes where material is readily mobilized by disturbance such as reimpacting ejecta. The area resurfaced by ejecta-induced flow is 50 times the area of Bralgah Crater.

Assuming the gravity regime, the main-belt velocities and the range of values in Table 1, the impactor that created Bralgah Crater

had a radius between 0.17 and 0.45 m. If we assume a strength of 2 Pa, the upper-bound radius increases only slightly to 0.6 m. By contrast, a 5.3 m radius would be required for the dry-soil strength of 0.18 MPa assumed in a previous analysis²⁰.

Impactor sizes relate to crater-retention age through the modelled impactor flux, which has a size-frequency distribution that varies approximately by the inverse cube of the impactor size³³. The 0.18 MPa assumption for surface strength yielded a crater-retention age of 0.1–1.0 Gyr in the main belt²⁰. If the surface strength is lower—even assuming our extreme upper bound, 100 Pa—the impactor flux would be 64 times higher (several per million years (ref. ²⁵)) and yield an age younger by the same factor. However, this simple scaling ignores several complicating factors, such as Bennu's transit from the main belt to near-Earth space³³ and the evidence of strength at depth in some locations ^{16,25,34} (see extended discussion in Methods). A single relationship between impactor sizes and crater diameters may not exist for rubble-pile asteroids, complicating analyses of crater-retention age.

Combining our findings with Hayabusa2's SCI experiment on Ryugu, we now have two measurements of negligible cohesive strength from craters of different diameters (70 versus 15 m) on two different rubble-pile asteroids. These data points from the only two such bodies to have been characterized in detail by spacecraft suggest a potentially broad applicability to rubble-pile surfaces. Even though the extremely weak uppermost layer may vary in thickness, our findings show that it must be considered when interpreting observations of rubble-pile asteroids, as is done in a companion paper²⁵ that estimates a range of crater-retention ages from the complete database of Bennu's craters.

Three implications of this work indicate that resurfacing is faster on low-gravity rubble piles than on larger and/or more cohesive asteroids. (1) Due to the low strength of regolith, craters are larger than predicted by models that assume higher strength, so the same impactor flux overturns more of the surface. Taking this into account leads to reduced estimates of crater-retention age²⁵. (2) Also due to the low strength, much of the crater material is ejected at velocities below the escape velocity, retaining the shock-comminuted material and contributing to crater infilling and other resurfacing. (3) With the high slopes available on fast-spinning asteroids, ejecta that return to the surface can easily mobilize material and create mass wasting that affects a larger area than the crater and ejecta-impact locations would alone. Given Bennu's estimated formation age of approximately 1 Gyr inferred from probable asteroid-source families in the main belt^{35,36}, Bennu has probably been resurfaced multiple times.

Online content

Any methods, additional references, Nature Research reporting summaries, source data, extended data, supplementary information, acknowledgements, peer review information; details of author contributions and competing interests; and statements of data and code availability are available at https://doi.org/10.1038/s41561-022-00937-y.

Received: 15 April 2021; Accepted: 25 March 2022; Published online: 23 May 2022

References

- Walsh, K. J. Rubble pile asteroids. Annu. Rev. Astron. Astrophys. 56, 593-624 (2018).
- Holsapple, K. A. The scaling of impact processes in planetary sciences. Annu. Rev. Earth Planet. Sci. 21, 333–373 (1993).
- Melosh, H. J. Impact Cratering: A Geologic Process (Oxford Monographs on Geology and Geophysics Series no. 11, Clarendon Press, 1989).
- Scheeres, D. J. Disaggregation of small, cohesive rubble pile asteroids due to YORP. *Icarus* 304, 183–191 (2018).

- Sugita, S. et al. The geomorphology, color, and thermal properties of Ryugu: implications for parent-body processes. Science https://doi.org/10.1126/ science.aaw0422 (2019).
- Lauretta, D. S. et al. The unexpected surface of asteroid (101955) Bennu. Nature 568, 55–60 (2019).
- Lauretta, D. S. in Sample Return Missions (ed. Longobardo, A.) 163–194 (Elsevier, 2021).
- 8. Rozitis, B. et al. Asteroid (101955) Bennu's weak boulders and thermally anomalous equator. Sci. Adv. 6, eabc3699 (2020).
- Ballouz, R. L. et al. Bennu's near-Earth lifetime of 1.75 million years inferred from craters on its boulders. *Nature* https://doi.org/10.1038/s41586-020-2846-z (2020).
- Arakawa, M. et al. An artificial impact on the asteroid 162173 Ryugu formed a crater in the gravity-dominated regime. Science https://doi.org/10.1126/ science.aaz1701 (2020).
- Rizk, B. et al. OCAMS: the OSIRIS-REx camera suite. Space Sci. Rev. 214, 26 (2018).
- Golish, D. R. et al. Ground and in-flight calibration of the OSIRIS-REx camera suite. Space Sci. Rev. 216, 12 (2020).
- 13. Bennett, C. A. et al. A high-resolution global basemap of (101955) Bennu. *Icarus* https://doi.org/10.1016/j.icarus.2020.113690 (2021).
- DellaGiustina, D. N. et al. Variations in color and reflectance on the surface of asteroid (101955) Bennu. Science https://doi.org/10.1126/science.abc3660 (2020).
- Barnouin, O. S. et al. Digital terrain mapping by the OSIRIS-REx mission. Planet. Space Sci. 180, 104764 (2020).
- Daly, R. T. et al. The morphometry of impact craters on Bennu. Geophys. Res. Lett. 47, e2020GL089672 (2020).
- Daly, M. G. et al. Hemispherical differences in the shape and topography of asteroid (101955) Bennu. Sci. Adv. 6, eabd3649 (2020).
- Jawin, E. R. et al. Global patterns of recent mass movement on asteroid (101955) Bennu. J. Geophys. Res. Planets 125, e2020JE006475 (2020).
- Takizawa, S. & Katsuragi, H. Scaling laws for the oblique impact cratering on an inclined granular surface. *Icarus* 335, 113409 (2020).
- Walsh, K. J. et al. Craters, boulders and regolith of (101955) Bennu indicative of an old and dynamic surface. Nat. Geosci. 12, 242–246 (2019).
- Scheeres, D. J. et al. The dynamic geophysical environment of (101955)
 Bennu based on OSIRIS-REx measurements. Nat. Astron. 3, 352–361 (2019).
- Chesley, S. R. et al. Trajectory estimation for particles observed in the vicinity of (101955) Bennu. J. Geophys. Res. Planets 125, e2019JE006363 (2020).
- Housen, K. R., Schmidt, R. M. & Holsapple, K. A. Crater ejecta scaling laws: fundamental forms based on dimensional analysis. *J. Geophys. Res.* 88, 2485–2499 (1983).
- Housen, K. R. & Holsapple, K. A. Ejecta from impact craters. *Icarus* 211, 856–875 (2011).
- Bierhaus, E. B. et al. Crater population on asteroid (101955) Bennu indicates impact armouring and a young surface. *Nat. Geosci.* https://doi.org/10.1038/ s41561-022-00914-5 (2022).
- Slyuta, E. N. Physical and mechanical properties of the lunar soil (a review). Sol. Syst. Res. 48, 330–353 (2014).
- 27. Barnouin, O. S. et al. Shape of (101955) Bennu indicative of a rubble pile with internal stiffness. *Nat. Geosci.* **12**, 247–252 (2019).
- Honda, R. et al. Resurfacing processes on asteroid (162173) Ryugu caused by an artificial impact of Hayabusa2's Small Carry-on Impactor. *Icarus* 366, 114530 (2021).
- McCaffrey, W. D. (ed.) Particulate Gravity Currents Vol. 31 (Blackwell Science, 2001).
- 30. Iverson, R. M. The physics of debris flows. Rev. Geophys. 35, 245-296 (1997).
- 31. Lauretta, D. S. & the OSIRIS-REx TAG team. The OSIRIS-REx touch-and-go sample acquisition event and implications for the nature of the returned sample. In *Proc. 52nd Lunar and Planetary Science Conference LPI* contribution no. 2548, abstract no. 2097 (2021).
- Vokrouhlický, D., Bottke, W. F., Chesley, S. R., Scheeres, D. J. & Statler, T. S. in Asteroids IV (eds Michel, P. et al.) 509–531 (Univ. Arizona Press, 2015).
- 33. Bottke, W. F. et al. Interpreting the cratering histories of Bennu, Ryugu, and other spacecraft-explored asteroids. *Astron. J* 160, 14 (2020).
- Roberts, J. H. et al. Rotational states and shapes of Ryugu and Bennu: implications for interior structure and strength. *Planet. Space Sci.* 204, 105268 (2021).
- Bottke, W. F. et al. In search of the source of asteroid (101955) Bennu: applications of the stochastic YORP model. *Icarus* 247, 191–217 (2015).
- Walsh, K. J., Delbo, M., Bottke, W. F., Vokrouhlicky, D. & Lauretta, D. S. Introducing the Eulalia and new Polana asteroid families: re-assessing primitive asteroid families in the inner Main Belt. *Icarus* 225, 283–297 (2013).

Publisher's note Springer Nature remains neutral with regard to jurisdictional claims in published maps and institutional affiliations.

 $\ensuremath{\mathbb{G}}$ The Author(s), under exclusive licence to Springer Nature Limited 2022

Methods

Mapping and measurements. We mapped the ejecta blanket and flow field on a global OCAMS/PolyCam mosaic of Bennu with a pixel scale of ~5 cm pixel⁻¹ (ref. ¹³) (Fig. 1a) and on OCAMS/MapCam image ocams20190322t233553s104_map_iofl2pan_78685 (Fig. 1b), which was collected on 22 March 2019 and has a pixel scale of 0.29 m pixel⁻¹. Elevations, slopes and tilts are from stereophotoclinometry (SPC) shape models¹⁵. Tilt variation (Fig. 1c) for a facet is the 1σ standard deviation of tilts of facets within a 5 m radius. Tilt variations are from the SPC v.20 shape model; other elevations and slopes are from the SPC v.42 shape model. The *b'*/*v* band ratio map in Fig. 1d was extracted from the global map in ref. ¹⁴. The high-spatial-resolution local digital terrain models (DTMs) in Extended Data Figs. 2 and 3 are produced from OSIRIS-REx Laser Altimeter data^{15,37}.

Ejecta simulations. The high-fidelity numerical simulation (Fig. 3 and Extended Data Fig. 4) used Interactive Data Language (IDL) software to understand the ejecta patterns and mass deposition. The velocities and mass distribution of ejecta are derived from terrestrial experiments, and Bennu parameters are derived from OSIRIS-REx observations (Table 1 contains the values and equations used). The simulation assumes gravity-regime scaling and Bennu's current shape and rotation rate. Ejecta particles are launched in a uniform distribution around the edge of Bralgah Crater and tracked in inertial space until they contact Bennu's surface. On the basis of terrestrial testing, all particles are ejected at 45° from local surface with a uniform azimuthal distribution. Higher-order (two and above) gravity terms and mass concentrations are ignored as they have little effect on the modelled trajectories. The maximum ejection speed in the simulation is 8 cm s⁻¹. Higher-velocity particles have a low fraction of the total ejected mass, and they travel far from the crater because they approach escape velocity. During the time aloft, downslope ejecta underwent a 30 m drift westwards due to Bennu's rotation. The crater formed slowly over 20 minutes, which was also the time aloft for most of the ejecta that returned to the surface. These parameterizations are based on crater diameter and are consistent with the outcome of the Hayabusa2 SCI experiment.

Applicability of gravity-regime scaling for Bennu's microgravity environment. Applying laboratory-based scaling relationships (Table 1) to Bennu necessitates extrapolating experimental results by several orders of magnitude. Nevertheless, the calculated ejection velocities are plausible and produce a feasible explanation for the ejecta field. These laboratory-based, point-source scaling relationships also proved relevant to full-scale experiments such as Deep Impact³⁸ and the SCI experiment¹⁰. Target compaction can suppress ejecta during impacts into porous targets³⁹, but the impactor creating Bralgah Crater was too small to cause compaction.

Other potential flow fields on Bennu. The terrain surrounding and north of Bralgah Crater is not unique: some smaller areas on Bennu have similar smoothness, dearth of larger rocks and comparable colours^{14,40}. These other regions contain finer material and include the interior of some craters and possible flow fields unassociated with craters but on higher slopes that cover smaller areas. Steepening of the slopes by increased rotation rate, a small impact or some other disturbance could have initiated an avalanche. Many of these regions are located near the same areas that have evidence of mass wasting surrounding large boulders¹⁸. Terraces are additional indicators that much of Bennu's surface material in the middle latitudes is near its stability limit^{17,27}. In the northern hemisphere, the apparent lower volume of fines may have limited the instances of flow fields despite the higher average slopes and a higher predominance of terraces.

Constraining surface strength. In the strength regime, ejection velocities at the crater edge are approximated by $v = C_3 \sqrt{Y/\rho}$, where *Y* is a measure of strength with dimensions of stress, ρ is the surface density, and C_3 is a fitted constant.

We constrain the possible strength by investigating several parameterizations and placing a value that is probably an extreme but that encloses many of the possible conditions. To set a maximum value on strength of the surface material ejected during formation of Bralgah Crater, we examine the slowest ejecta speeds, which increase as surface strength increases. The slowest ejecta are launched near the crater rim in the final stages of the cratering process. Using one crater radius as the distance that certainly contains ejecta, the minimum deduced ejecta speed is 3.5 cm s⁻¹, the speed required to land within one crater radius downslope. (There appear to be ejecta closer than one radius from the crater rim, so this is a maximum speed.) The solid lines in Extended Data Fig. 4a are the slowest available speeds using the equations for ejecta velocities in Table 1 for different material properties.

Unfortunately, the slowest ejecta speeds are poorly understood, particularly for low-strength material in microgravity, a regime not available for hypervelocity terrestrial experiments. A common treatment for these slowest speeds is to insert an empirically derived factor, $\left(1-\frac{x}{n_2R}\right)^p$, into the velocity equation to drive the velocities to zero near the crater edge rather than having the lowest possible speeds truncated at a non-zero value²⁴. Since ejecta mass is proportional to x^3 , this edge-modification factor affects the relationship between ejected mass and velocity, producing the results shown in Fig. 2b and Extended Data Fig. 4. Both gravity and strength regimes require this modification to the basic equations.

After adding this $\left(1-\frac{x}{n_2R}\right)^p$ factor, we need a different algorithm for finding the lowest velocity to constrain surface strength. We choose an approach based

on the total ejected mass: at least 5% of the ejected mass must be slower than the $3.5\,\mathrm{cm\,s^{-1}}$ velocity required to land within one crater radius of the rim. This approach—along with the parameterizations from laboratory experiments—produces the dashed lines in Extended Data Fig. 4a and increases the maximum possible strength to $100\,\mathrm{Pa}$.

The strength may in fact be much less, but that cannot be discerned from comparing the Bennu observations with the results of terrestrial testing.

Data availability

OCAMS data are available via the Planetary Data System (PDS) at https://sbn.psi.edu/pds/resource/orex/ocams.html⁴¹. The global image mosaic of Bennu is available in ref. ¹³. OLA data underlying the DTMs used for slope calculations are available via the PDS at https://sbn.psi.edu/pds/resource/orex/ola.html⁴². The v.42 global DTM is available from the Small Body Mapping Tool (SBMT) at https://sbmt.jhuapl.edu. The output of the ejecta simulations is archived at https://lib.jhuapl.edu/.

Code availability

The ejecta-simulation programmes are available at https://lib.jhuapl.edu/.

References

- Daly, M. G. et al. The OSIRIS-REx Laser Altimeter (OLA) investigation and instrument. Space Sci. Rev. 212, 899–924 (2017).
- Schultz, P. H., Ernst, C. M. & Anderson, J. L. B. Expectations for crater size and photometric evolution from the deep impact collision. *Space Sci. Rev.* 117, 207–239 (2005).
- Housen, K. R., Sweet, W. J. & Holsapple, K. A. Impacts into porous asteroids. Icarus 300, 72–96 (2018).
- Golish, D. R. et al. A high-resolution normal albedo map of asteroid (101955) Bennu. *Icarus* 355, 114133 (2020).
- Rizk, B., Drouet d'Aubigny, C., Golish, D., DellaGiustina, D. N. & Laurentta, D. S. Origins, Spectral Interpretation, Resource Identification, Security, Regolith Explorer (OSIRIS-REx): OSIRIS-REx Camera Suite (OCAMS) Bundle (NASA Planetary Data System, 2019).
- Daly, M., Barnouin, O., Espiritu, R. & Lauretta, D. Origins, Spectral Interpretation, Resource Identification, Security, Regolith Explorer (OSIRIS-REx): OSIRIS-REx Laser Altimeter Bundle (NASA Planetary Data System, 2019).

Acknowledgements

This material is based on work supported by NASA under contracts NNM10AA11C and NNG12FD66C, issued through the New Frontiers Program. The OSIRIS-REx Laser Altimeter and the Canadian authors were supported by the Canadian Space Agency. P.M. acknowledges funding support from the French space agency CNES, from the European Union's Horizon 2020 research and innovation programme under grant agreement no. 870377 (project NEO-MAPP) and from Academies of Excellence: Complex systems and Space, environment, risk, and resilience, part of the IDEX JEDI of the Université Côte d'Azur. This work used the Small Body Mapping Tool (http://sbmt.jhuapl.edu). We are grateful to C. Wolner for her indispensable editing support and to the entire OSIRIS-REx Team of engineers, operators, scientists and administrators for making the encounter with Bennu possible.

Author contributions

M.E.P. led the data analysis and writing. O.S.B. led the Altimetry Working Group that produced the DTMs. O.S.B., R.T.D. and C.M.E. contributed analyses and expertise on crater processes. M.G.D. and J.A.S. provided the altimetry data for the high-resolution DTMs. E.B.B. and R.-L.B. provided analyses on crater-retention age. K.J.W., M.C.N. and P.M. contributed to writing. D.N.D. and D.R.G. provided image and spectral analyses. J.P.E., M.M.A., E.R.J., W.E.B. and C.L.J. provided analytical insight. D.S.L. is principal investigator of the OSIRIS-REx mission.

Competing interests

The authors declare no competing interests.

Additional information

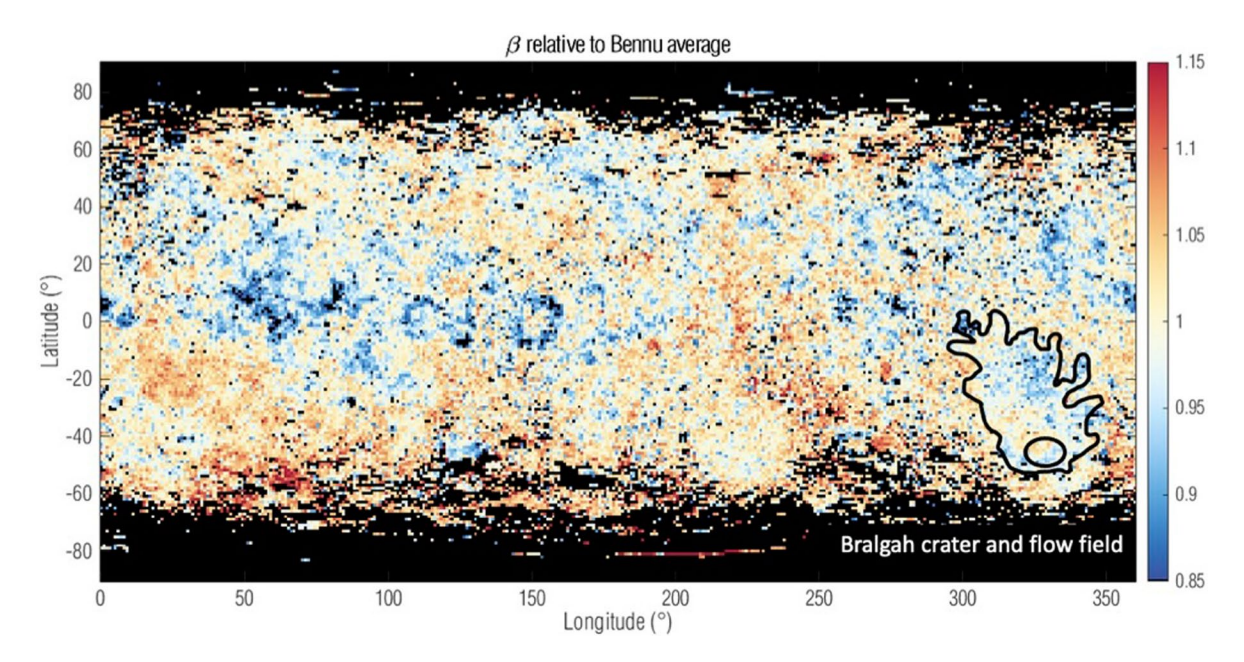
Extended data is available for this paper at https://doi.org/10.1038/s41561-022-00937-y.

Supplementary information The online version contains supplementary material available at https://doi.org/10.1038/s41561-022-00937-y.

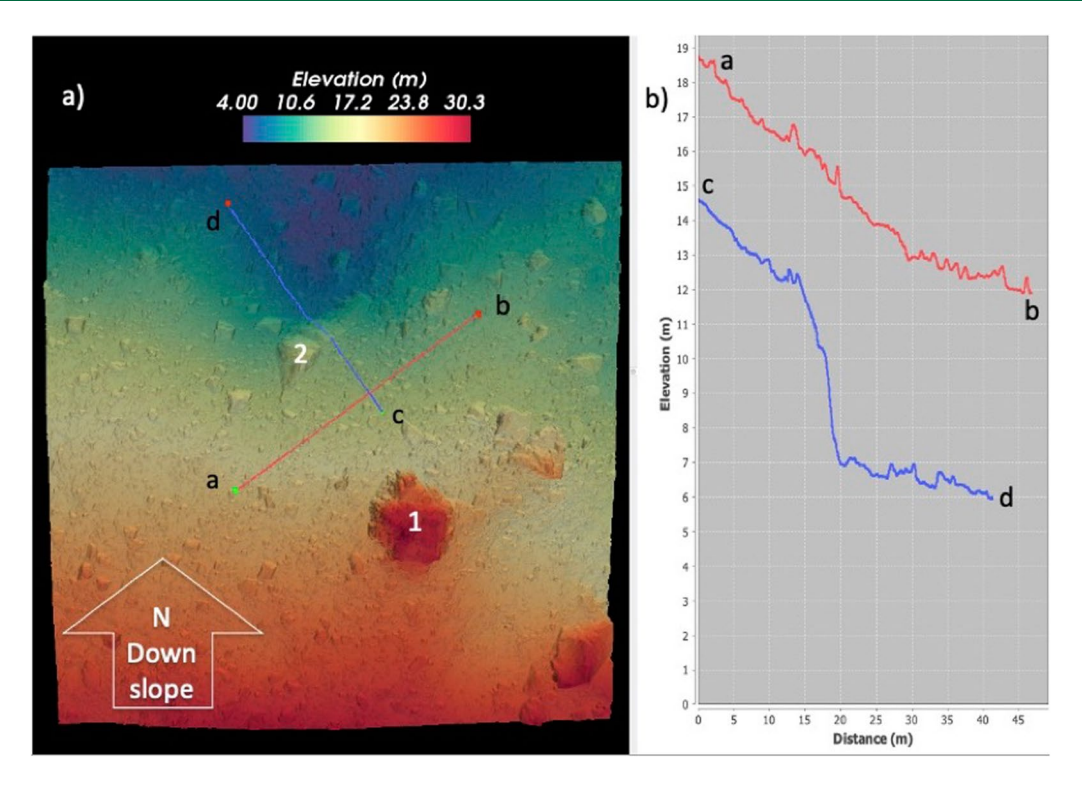
Correspondence and requests for materials should be addressed to M. E. Perry.

Peer review information Nature Geoscience thanks Akbar Whizin, Jennifer Anderson and the other, anonymous, reviewer(s) for their contribution to the peer review of this work. Primary Handling Editors: Tamara Goldin and James Super, in collaboration with the Nature Geoscience team.

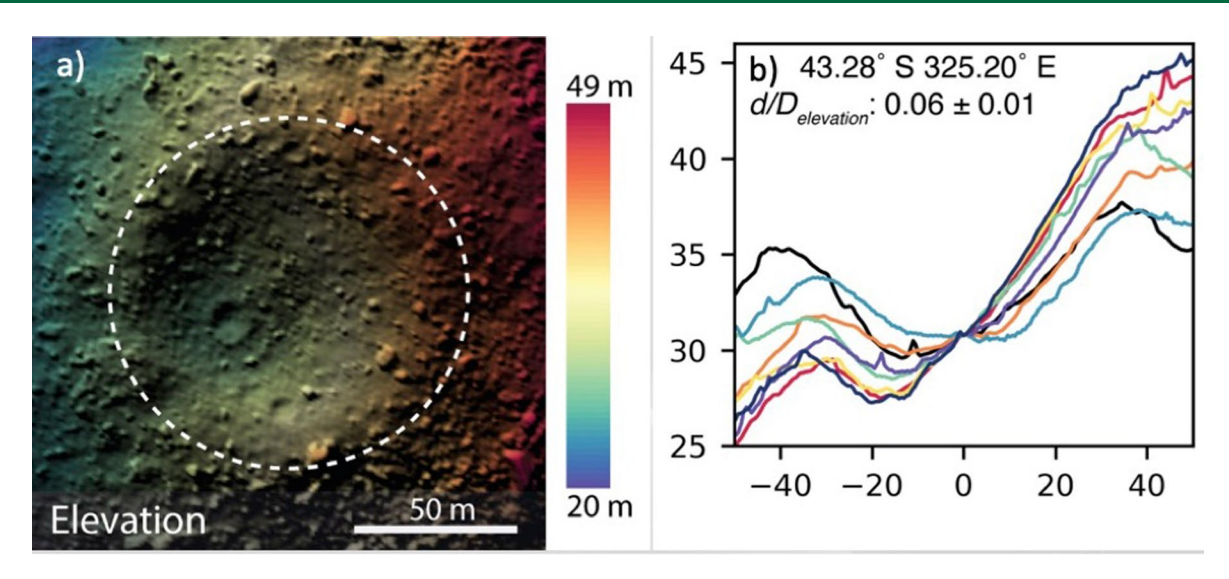
Reprints and permissions information is available at www.nature.com/reprints.



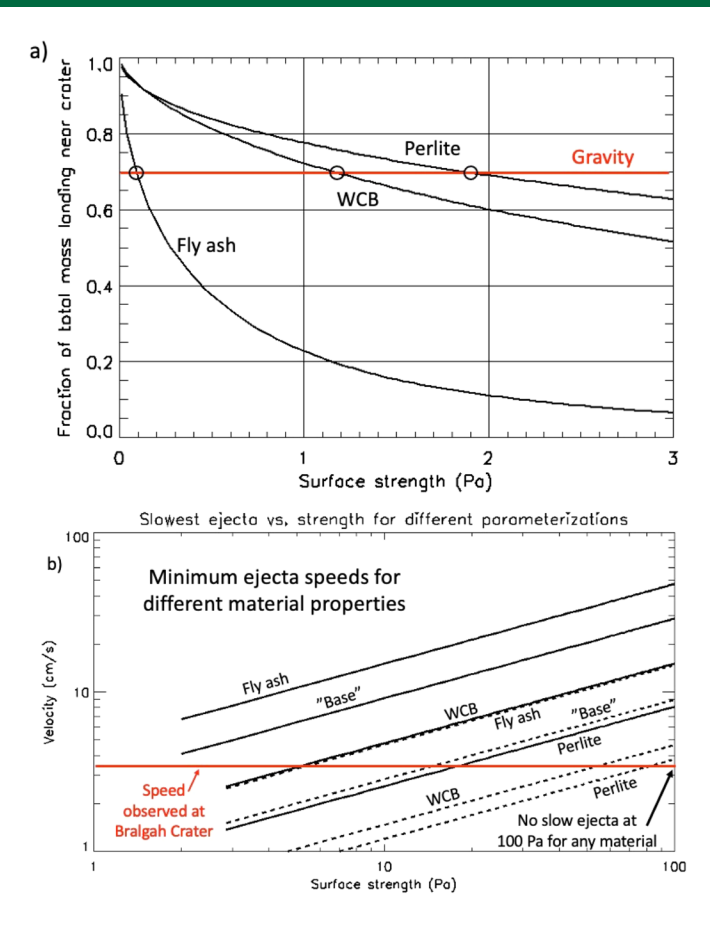
Extended Data Fig. 1 Color-phase slope of Bennu's surface. The colors are the phase slope (Golish et al. 2021) from the linear (in magnitude space) phase function, averaged over 1 degree and normalized to the Bennu average. The underlying data are the PolyCam albedo basemap (Golish et al. 2021). Notionally, low phase slope values (blue) indicate a smoother surface. The blue area north of Bralgah Crater is centered at -45°, 325° E. The scale is -10%/+5%, so the flow region is approximately a 10% effect in the phase slope.



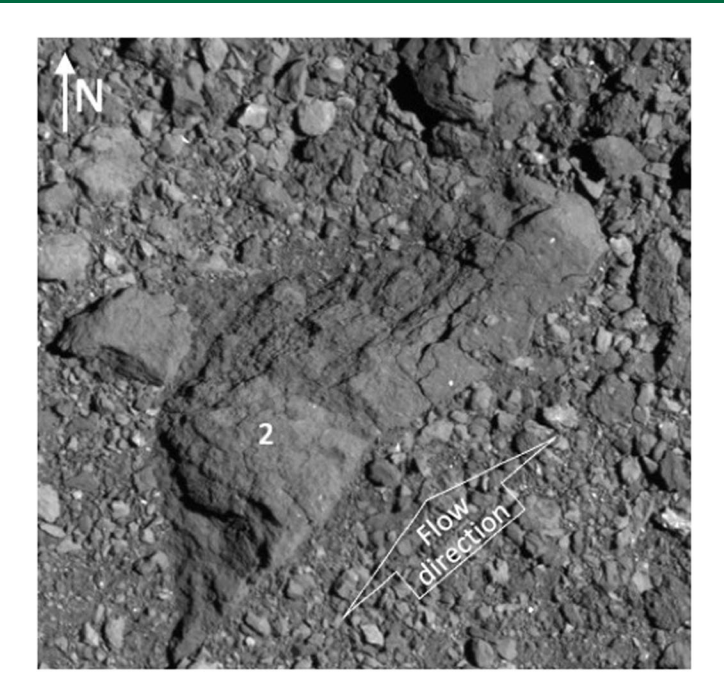
Extended Data Fig. 2 | Laser altimetry topography of the flow field around boulder 2. Laser altimetry topography of the flow field around boulder 2 showing elevations 4 to 5 m lower behind (north) of the bolder. The blue and red lines shown in **a** correspond to the profiles in **b**.



Extended Data Fig. 3 | Topography of Bralgah Crater from laser altimetry data. Topography of Bralgah Crater from laser altimetry data (Figs. 1, 2) 16 . **a**, DTM overlaid onto an OCAMS image (ocams20190419t204556s223_map_iofl2pan_92585). North (downslope) is to the left. **b**, Eight profiles of the crater. The value $d/D_{\text{elevation}}$ is crater depth (calculated from elevation) divided by crater diameter. The apparent asymmetry is due to the prevailing ~23° slope of the local region. Because of compaction and uplift near the crater rim, the total volume of material excavated from an impact crater is typically about 2/3 of the crater volume^{24,37}.



Extended Data Fig. 4 | Ejecta mass and velocity as a function of target strength. Calculations of ejecta velocities and the resulting ejected mass using the equations in Table 1 and published parameters²⁴ for three different low-strength material analogs for Bennu's regolith. WCB is weakly cemented basalt, and 'Base' has the constant C_3 =1 in the strength equation for ejection velocity. **a**, Fraction of ejecta landing within one crater radius of Bralgah as a function of target strength for the three different types of low-strength materials. The red line represents the fraction for gravity-regime scaling. The highest strengths that produce as much low-velocity ejecta as in the gravity regime are 0.1, 1.2, and 1.9 Pa (marked with circles). We consider this the range of possible strengths for Bennu's regolith. **b**, The minimum ejection velocity for the different strength parameterizations. The red line represents the lowest observed speed based on ejecta as close as 1 crater radius from the rim. The solid lines use the Table-1 equations, and the dashed lines include an additional factor that assumes ejecta velocities are not truncated and must smoothly approach zero. Although many of the potential surface properties do not have sufficiently slow velocities at 20 Pa, all of the strength parameterizations have high velocities at 100 Pa.



Extended Data Fig. 5 | Higher-resolution view of boulder 2 showing more material on the side of the boulder facing the flow. Higher-resolution view (global mosaic¹³) of boulder 2 showing more material on the side of the boulder facing the flow. This indicates that material flowed against the south-east side of the boulder. Extended Data Fig. 2 shows the drop in elevation to the northwest.

Extended Data Table 1 | Fitted parameters used for analyses and simulations²⁴

	Gravity		Strength	Strength					
Parameter	Dry sand	GMS	Fly ash	Base	WCB	Perlite			
μ	0.41	0.45	0.4	0.4	0.46	0.35			
ν	0.4	0.4	0.4	0.4	0.4	0.4			
<i>C</i> ₁	0.55	1.0	0.55	0.5	0.18	0.6			
k	0.3	0.5	0.3	0.3	0.3	0.32			
H_1	0.59	0.8	NA						
H_2		NA	0.4	0.4	0.38	0.81			
C_4	Calculated from k, mu, and C1: C4= 3.0 *k/ 4.0 /pi*C1^(3.0 *mu)								
n_2	1.3	1.3	1.0	1.0	1.0	1.0			
р	0.3	0.3	0.3	0.3	0.3	0.2			

WCB= weakly cemented basalt; Fly ash= sand/fly ash mixture; Perlite= Perlite/sand mixture; GMS= Glass microspheres. Data are from Housen and Holsapple, 2011, Table 3.